INELASTIC CYCLIC BEHAVIOR OF REINFORCED CONCRETE FLEXURAL MEMBERS

Bilgin Atalay[I] and Joseph Penzien[II]

SYNOPSIS

Presented is a mathematical model for predicting the force-deformation characteristics of reinforced concrete flexural members under inelastic cyclic conditions [1].

INTRODUCTION

Considering a reinforced concrete frame, the established philosophy of earthquake resistant design necessitates localized inelastic deformations occurring at certain overstressed regions designated as critical regions. Four series of tests have been conducted at the University of California, Berkeley [1,2,3,4] to study the flexural hysteretic behavior of critical regions under various combinations of internal force components controlling their behavior. The results of the series of tests reported in reference [1] in particular, permit the formulation of a mathematical model. The geometry and reinforcing details of a typical test specimen of this series is shown in Fig. 1.

INELASTIC HYSTERETIC BEHAVIOR

To formulate an appropriate mathematical model for reinforced concrete members subjected to cyclic inelastic deformations under combined moment, shear, and axial force, the lateral force-displacement behavior must be modelled realistically; i.e. one must be able to obtain the lateral force time history corresponding to a controlled lateral displacement time history.

Suppose for example, the lateral displacement time history of a member is that function shown in Fig. 2.a. The corresponding lateral force-displacement relation will be very similar to that shown by the solid line in Fig. 3. Knowing these two relations, the lateral force time history can be obtained as shown in Fig. 2.b.

In modelling the force-displacement relation of a member under constant axial load, one should first establish the so called "skeleton" curve. This curve is defined as the lateral force-displacement relation under separate but independent positive and negative monotonically increasing lateral displacements. Referring to Fig. 3, if the member under constant axial load is initially subjected to a positive monotonically increasing lateral displacement, the lateral load will increase "elastically" to point M, remain at essentially a constant value F_y under yielding conditions to point Q, and then will drop off along line QS showing a decrease in strength with increasing displacement beyond δ_N. This decrease is due primarily to crushing and spalling of the concrete cover on the compression sides of the member in the critical region. If instead the member under the same axial load had initially been subjected to a negative monotonically increasing lateral displacement, the lateral load would change along curve OM'Q' and then drop off with further increases in lateral displacement along line Q'S'. The force-displacement

[I] Research Assistant, University of California, Berkeley

[II] Professor of Structural Engineering, University of California, Berkeley

relations under these two monotonic conditions combine to form the basic skeleton curve S'Q'M'OMQS.

Let us now examine in more detail the force-displacement relation shown in Fig. 3 for cyclic loading. If initially, cyclic loading should take place at amplitudes in the range $-\delta_y < \delta < \delta_y$, the member will remain "elastic" and the corresponding force-displacement time history will be along line MM'. However as soon as the lateral displacement exceeds the yield level, hysteretic inelastic response follows with each subsequent cycle of deformation. In Fig. 3, the yield level is first exceeded at point M' with the displacement continuing to a value δ_1 as shown at point P'. The displacement then reverses and continues to δ_2 along curve P'MP (J = 1) which constitutes the first full half-cycle of deformation following initial yielding of the member. Again reversing the lateral displacement and continuing to δ_3 along curve PP'Q'R' (J = 2), the second full half-cycle of deformation is completed. Had this particular half-cycle terminated at point P' rather than R', continuing repeated cycles of deformation from δ_1 to δ_2 and back to δ_1 would produce stable hysteretic loops connecting points P and P'. Such stable behavior is experienced provided the absolute values of δ_1, δ_2, and all previous displacements have not exceeded δ_N and provided the shear stresses are relatively low. The third full half-cycle of deformation in Fig. 3 starts at point R', proceeds along curve J = 3 to point T, and then follows the skeleton curve to point R where the deflection equals δ_4. Note that at deflection δ_2 along this curve, the lateral force is somewhat reduced from the value F_y experienced on the previous half-cycle as represented by point P. Such a reduction at a fixed amplitude is experienced when the previous deformation time history has exceeded $\delta = \pm \delta_N$. This represents unstable hysteretic behavior which follows with each subsequent half-cycle as shown by curves J = 4,5,6,7 and 8. Note that quantities J, δ_J, t_J and F_J shown in Figs. 2, 3 and 4 refer to the number of inelastic half-cycles following initial yielding, the displacement at the initial point of the Jth inelastic half-cycle, time at the initial point of the Jth inelastic half-cycle, and the lateral force at the initial point of the Jth inelastic half-cycle, respectively.

Three important characteristics of inelastic cyclic behavior become apparent (1) the reduction in overall (or average) stiffness with increasing amplitudes of inelastic deformation beyond $\delta = \pm \delta_y$, (2) the reduction in lateral resistance at a fixed displacement with each repeated full half-cycle of inelastic deformation beyond $\delta = \pm \delta_N$, and (3) the shape of the hysteretic loops as influenced by certain member parameters and loading conditions. It is important when formulating an appropriate mathematical model that these characteristics be represented in a realistic manner. To be practical however this model must be easily adapted to numerical procedures. Therefore, a proper balance must be maintained between simplicity and accuracy.

FORM OF MATHEMATICAL MODEL

To formulate an appropriate force-deflection mathematical model, an analytical expression must be developed which will characterize the Jth inelastic half-cycle (J = 1,2,...) starting at time t_J. Since in applications, the extent of the Jth half is not known prior to its occurrence, this expression must be formulated knowing only the initial point (δ_J, F_J) representing $t = t_J$ and the previous force-deflection time history.

To accomplish this, a function $F_J(\delta)$ will be written as shown in Table 1 which passes through the known initial point (δ_J,F_J), designated here as point A, and an index point B whose location reflects the influence of the

member's force-deflection time history prior to $t = t_J$. The deflection at point B, designated as δ_J^M, is the maximum deflection which occurred prior to $t = t_J$ for half-cycles of increasing deflection and is the minimum deflection which occurred prior to $t = t_J$ for half-cycles of decreasing deflection; see Eq. (1).

TABLE 1: RELATIONS CONTROLLING THE Jth INELASTIC HALF-CYCLE

	HALF CYCLES OF INCREASING DEFLECTION, i.e. J=1,3,5,...1F INITIAL YIELD IN (-) DIRECTION, $F_1=-F_y$ J=2,4,6,...1F INITIAL YIELD IN (+) DIRECTION; $F_1=+F_y$	HALF CYCLES OF DECREASING DEFLECTION, i.e. J=2,4,6,...1F INITIAL YIELD IN (-) DIRECTION; $F_1=-F_y$ J=1,3,5,...1F INITIAL YIELD IN (+) DIRECTION: $F_1=+F_y$	
δ_J^M † =	Max. $\{\delta(t)\}$; $0 < t < t_J$	Min. $\{\delta(t)\}$; $0 < t < t_J$	(1)
F_J^M † =	$F_J^P - \Delta F_{J-1} - \Delta F_J$	$F_J^P + \Delta F_{J-1} + \Delta F_J$	(2)
$F_J(\delta)$ =	$F_J+K_J(\delta-\delta_J)+A_J\cos\frac{\pi}{2}\left[\frac{2\delta-\delta_J^M-\delta_J}{\delta_J^M-\delta_J}\right] - B_J\left(\frac{1}{2}+\frac{1}{2}\cos\frac{\pi\delta}{\delta_{PJ}}\right)$; $\delta_{PJ} < 0$, $\delta_{PJ} \le \delta \le -\delta_{PJ}$	$F_J+K_J(\delta-\delta_J)-A_J\cos\frac{\pi}{2}\left[\frac{2\delta-\delta_J^M-\delta_J}{\delta_J^M-\delta_J}\right]+B_J\left(\frac{1}{2}+\frac{1}{2}\cos\frac{\pi\delta}{\delta_{PJ}}\right)$; $\delta_{PJ} > 0$, $-\delta_{PJ} \le \delta \le \delta_{PJ}$	(3)
	$F_J+K_J(\delta-\delta_J)+A_J\cos\frac{\pi}{2}\left[\frac{2\delta-\delta_J^M-\delta_J}{\delta_J^M-\delta_J}\right]$; $\delta_{PJ}<0$, $\delta\le\delta_{PJ}$, $\delta>-\delta_{PJ}$	$F_J+K_J(\delta-\delta_J)-A_J\cos\frac{\pi}{2}\left[\frac{2\delta-\delta_J^M-\delta_J}{\delta_J^M-\delta_J}\right]$; $\delta_{PJ}>0$, $\delta\le-\delta_{PJ}$, $\delta\ge\delta_{PJ}$	(4)
	$\delta_{PJ}>0$, $-\infty < \delta < \infty$	$\delta_{PJ}>0$, $-\infty < \delta < \infty$	

† EXCEPT $\delta_1^M \equiv \delta_y$ & $F_1^M \equiv F_y$ if $F_1 = -F_y$

$\delta_1^M \equiv -\delta_y$ & $F_1^M \equiv -F_y$ if $F_1 = +F_y$

The lateral force at point B, designated as F_J^M, is given by Eq. (2) where F_J^P is equal to instantaneous lateral force which was present when $\delta(t)$ last reached the value δ_J^M as defined by Eq. (1) and where ΔF_{J-1} and ΔF_J are positive quantities representing resistance losses due to possible unstable hysteretic behavior during half-cycles J-1 and J, respectively. Each of these losses exist only if the deflection time-history during or prior to the half-cycle represented has exceeded + δ_N or - δ_N. The inelastic half-cycles for J = 1 through J = 8 in Fig. 3 are separated and shown again in Fig. 4. The initial point A, the index point B, and the terminal point C is shown for each half-cycle.

In formulating function $F_J(\delta)$, it is convenient to use the slope of the straight line passing through points A and B, i.e. $K_J \equiv (F_J^M-F_J)/(\delta_J^M-\delta_J)$, J=1,2,3,···. This function, with certain restrictions on its use, can be expressed by the approximate empirical Eqs. (3) and (4), Table 1. Quantities A_J and B_J appearing in Eqs. (3) and (4) are positive coefficients. Quantity δ_{PJ} appearing in Eq. (3) and in the conditional relations is that value of δ which yields a zero value for $F_J(\delta)$ using Eq. (4).

The first two terms on the right hand side of Eqs. (3) and (4) express the equation of the straight line passing through points A and B while the remaining two terms in Eq. (3) and the single remaining term in Eq. (4) represent the deviation of the function $F_J(\delta)$ from this straight line. The last term in Eq. (3) containing the coefficient B_J represents the pinched form of the hysteretic loop. Implicit in the form of this last term is the simplifying assumption that the pinched form is symmetric with respect

to $\delta = 0$. This assumption is, of course, not strictly true.

Function $F_J(\delta)$ as defined by Eqs. (3) and (4) can represent the entire Jth half-cycle only when it stays within certain bounds of the skeleton curve $F_S(\delta)$; i.e. the function $F_J(\delta)$ must never be extended across the skeleton curve for $|\delta| > \delta_y$. For example in Fig. 3, while half-cycles J = 4 through J = 8 can be represented entirely by Eqs. (3) and (4), half cycles J = 1 through J = 3 can only be partly represented by these equations. Function $F_J(\delta)$ as defined by Eqs. (3) and (4) represents half-cycles J = 1, J = 2, and J = 3 from their initial points to points M, P', and T, respectively. The remaining portions of these half-cycles, namely portions MP, P'Q'R', and TQR, must follow the skeleton curve . Mathematically this means that when $F_J(\delta)$ as defined by Eqs. (3) and (4) satisfies the condition

$$|F_J(\delta)| < |F_S(\delta)| \qquad \delta < -\delta_y \; ; \; \delta > \delta_y \; ; \; J = 1,2,... \tag{5}$$

it is applicable. However, when Eqs. (3) and (4) do not satisfy Eq. (5), it is not applicable in which case $F_S(\delta)$ should be used for $F_J(\delta)$. Obviously therefore, the skeleton curve must be represented in mathematical terms. Referring to Fig. 3, this relation can be expressed in the form

$$F_S(\delta) = \begin{cases} \dfrac{F_y}{\delta_y}\delta & -\delta_y \le \delta \le \delta_y \\ F_y & \delta_y \le \delta \le \delta_N \\ -F_y & -\delta_N \le \delta \le -\delta_y \\ F_y\left[1 - \beta_S\left(\dfrac{\delta_y}{\delta_N} - \dfrac{\delta_y}{\delta}\right)\right] & \delta \ge \delta_N \\ -F_y\left[1 - \beta_S\left(\dfrac{\delta_y}{\delta_N} + \dfrac{\delta_y}{\delta}\right)\right] & \delta \le -\delta_N \end{cases} \tag{6}$$

where β_S is a positive scalar factor.

Parameters δ_N, β_S, ΔF_J, A_J, and B_J appearing in the above relations which formulate the overall mathematical model must be obtained from experimental evidence. Having their numerical values along with the numerical values for F_y and δ_y, the Jth inelastic half-cycle is completely defined. Once the Jth half-cycle is complete, its terminal point becomes the initial point for the J+1 half-cycle. One defines this half-cycle in exactly the same manner used for the Jth half-cycle. By this method, one can obtain the entire force-displacement time history.

EVALUATION OF PARAMETERS IN MATHEMATICAL MODEL

The parameters of the mathematical model presented in the previous section can be identified as F_y, δ_y, δ_N, β_S, ΔF_J, A_J, and B_J. Based on experimental data corresponding to a specimen with geometry and reinforcement detailing shown in Fig. 1, empirical relations have been formulated for their

numerical evaluation.

Factors F_y and δ_y - Numerical values for lateral force and displacement at initial yield, F_y and δ_y can normally be obtained through analytical methods of structural analysis.

Factor δ_N - The lateral displacement at initiation of loss of lateral resistance, δ_N can be evaluated using the empirical relation

$$\frac{\delta_y}{\delta_N} = 0.05 + 2.58\ \eta_o \tag{7}$$

where $\eta_o = N/bD\ f'_c$ is an axial compression index.

Factor β_s - Factor β_s is a measure of the loss of lateral resistance due to increasing lateral displacement, and as shown by experimental results, is a function of applied axial load, N, and transverse reinforcement spacing, s. Its value can be estimated using the empirical relation

$$\beta_s = 0.27 - 0.045\ \frac{d}{s} + \left(2.92 - 0.49\ \frac{d}{s}\right)\eta_o \tag{8}$$

Factor ΔF_J - For displacement amplitudes less than $\pm\ \delta_N$, there is no loss in resistance over a full half-cycle of deformation; therefore,

$$\Delta F_J = 0 \qquad \text{max.}\ \{|\delta(t)|\} \le \delta_N \qquad 0 < t < t_J \tag{9}$$

For displacement amplitudes greater than $\pm\ \delta_N$ a loss in resistance does occur which can be approximated by the relation

$$\Delta F_J = [0.15\ \eta_o^2 + 0.002(3.33 - \frac{d}{s})]F_y \qquad \delta_M > \text{max.}\{|\delta(t)|\} > \delta_N \qquad 0 < t < t_J \tag{10}$$

Displacement δ_M is that value of δ beyond which the loss in resistance per full half-cycle ΔF_J becomes significantly larger than that given by Eq. (10).

Factors A_J and B_J - An analysis of experimental results shows that simple empirical relationships can be used in the estimation of factors A_J and B_J, namely:

$$\frac{A_J}{F_y} = -0.17 + (0.27 + 0.30\ \eta_o)\ \mu_J - (0.02 + 0.04\ \eta_o)\mu_J^2 \qquad \mu_J \ge 1 \tag{11}$$

and

$$\frac{B_J}{F_y} = \left(0.245 - 0.284\ \eta_o - 0.008\ \frac{d}{s}\right)\left(\mu_J - 1\right)^{1/2} \qquad \mu_J \ge 1 \tag{12}$$

The quantity μ_J appearing in Eqs. (11) and (12) is the cyclic lateral displacement ductility factor defined as:

$$\mu_J = \frac{|\delta_J^M - \delta_{J-1}^M|}{2\delta_y} \tag{13}$$

Factor B_J reflects the amount of "pinching", or the reduction of

instantaneous shear stiffness near zero lateral load. It is well established (see), for example [3]) that this reduction in stiffness is an inverse function of a/D, the moment arm-to-depth ratio. Since in the present experimental investigation only one a/D ratio (fairly high to prevent shear type failures) was used, the effect of this ratio is not apparent in Eq. (12); therefore, it is suggested that the quantity B_J/F_y be increased properly for decreasing values of a/D.

CONCLUDING STATEMENT

The mathematical model presented in the preceeding sections can be checked against the experimental test data using a specially developed computer program. An example lateral force-displacement relationship calculated through the use of the mathematical model is presented graphically in Fig. 5. Only the relationships corresponding to the first and last half cycles of lateral loading at a lateral displacement amplitude in the inelastic range are duplicated. The mathematical model reproduces satisfactorily the important response characteristics pertinent to inelastic cyclic behavior. As evidence of the simplicity of the mathematical model it is worth noting that the calculations needed to generate the lateral force-displacement diagrams for 6 specimens, each with a different combination of applied axial load and transverse reinforcement spacing and each containing about 40 half cycles of loading, required about 3 seconds of central processor time in the CDC-6400 computer.

ACKNOWLEDGMENT

The authors acknowledge the financial support provided by the National Science Foundation through Grant No. AEN73-07732 A02.

REFERENCES

[1] Atalay, B., and Penzien, J., "The Seismic Behavior of Critical Regions of Reinforced Concrete Components as Influenced by Moment, Shear, and Axial Force," EERC 75-19, Earthquake Engineering Research Center, University of California, Berkeley, 1975.

[2] Bertero, V. V., Bresler, B., and Liao, H., "Stiffness Degradation of Reinforced Concrete Structures Subjected to Reversed Actions," EERC 69-12, Earthquake Engineering Research Center, University of California, Berkeley, 1969.

[3] Mahin, S., Bertero, V. V., Rea, D., and Atalay, B., "Rate of Loading Effects on Uncracked and Repaired Reinforced Concrete Members," EERC 72-9, Earthquake Engineering Research Center, University of California, Berkeley, 1972.

[4] Celebi, M., and Penzien, J., "Experimental Investigation into the Seismic Behavior of Critical Regions of Reinforced Concrete Components as Influenced by Moment and Shear," EERC 73-4, Earthquake Engineering Research Center, University of California, Berkeley, 1973.

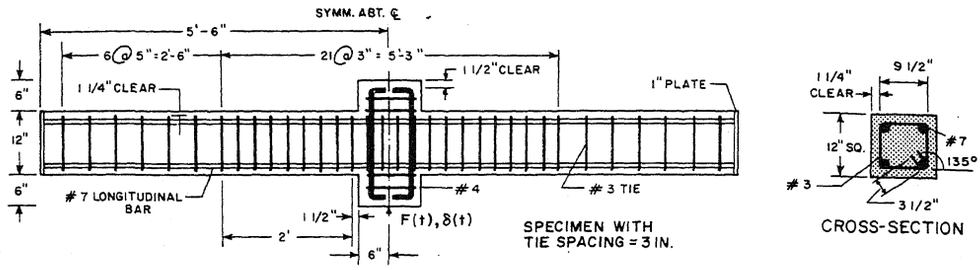

Fig. 1. Test Specimen Geometry and Reinforcement Details

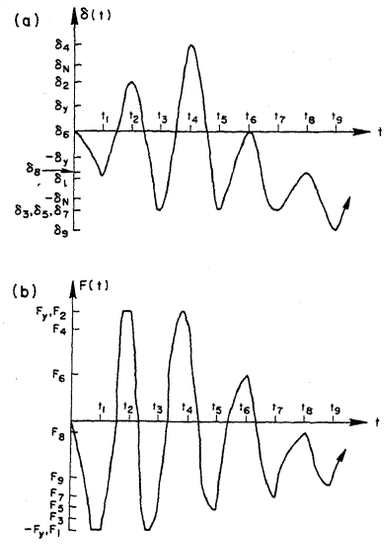

Fig. 2. Example Lateral Displacement-Time and Corresponding Lateral Force-Time Histories

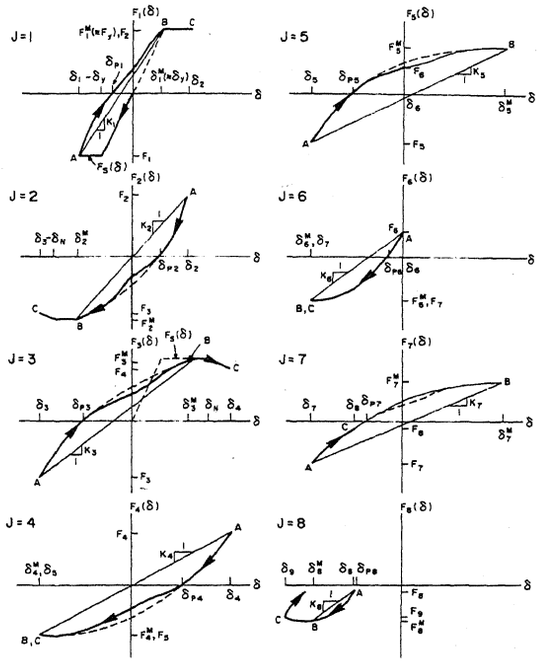

Fig. 4. Lateral Force-Displacement Relations for Inelastic Half Cycles of Loading

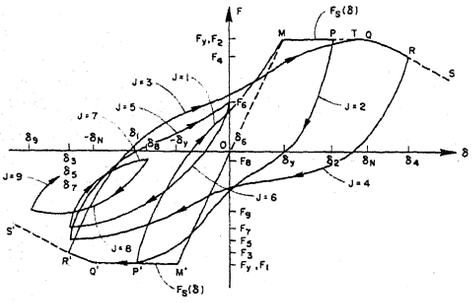

Fig. 3. Example Lateral Force-Displacement Relation

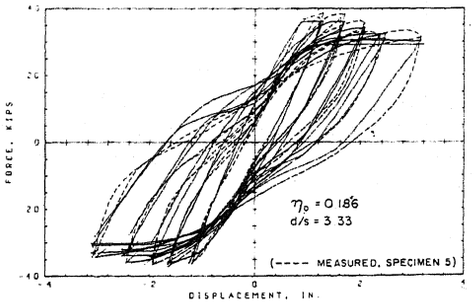

Fig. 5. Calculated Lateral Force-Displacement Relationship